

Numerical Simulation of RCCS under LPCC Accident in PMR600 Using CFD

Seong Hoon Kim^{a*}, Nam-il Tak^a, Min-Hwan Kim^a

^aKorea Atomic Energy Research Institute, 150 Deokjin-dong, Yuseong-gu, Daejeon 305-353, Korea

*Corresponding author: shkim822@kaeri.re.kr

1. Introduction

The Reactor Cavity Cooling System (RCCS) is the ultimate heat sink of the core decay heat under accident conditions. RCCS has a capability to limit the reactor pressure vessel temperature under the design safety limit following accidents such as High Pressure Conduction Cooling (HPCC) and Low Pressure Conduction Cooling (LPCC). The initiating event for LPCC is the guillotine rupture of a coaxial pipe or a simultaneous break of all the connecting pipes between the reactor pressure vessel and the heat transport system. A simulation for LPCC accident of PMR600 was conducted by using the GAMMA+ code [1].

The GAMMA+ code, which is developed to analyze the thermo-fluid transients in HTGR, is a system code and it treats the momentum and energy transfer differently from the computational fluid dynamics (CFD). There might exist the difference between the estimations using GAMMA+ and CFD.

In a previous study [2] the steady state performance of RCCS in HTGR (High Temperature Gas-Cooled Reactor) was calculated using the computational fluid dynamics with the porous medium approach and the axisymmetric assumption. Even though this assumption reduces the computational time significantly, it changes the RCCS tube shape. This may change the behavior of RCCS. In this study, we develop three candidates of RCCS for CFD, conduct the unsteady simulations for the LPCC accident, and compare the results with the GAMMA+ code. By doing this, we can find a suitable model for RCCS when CFD is conducted with the axisymmetric assumption.

2. Methods and Results

2.1 Computational Domain and Methods

Three axisymmetric models were created for the simulation. Total number of the grids for each model is 44000. Figure 1 shows the computational domains used for the simulation. The computational domains consist of the reactor pressure vessel (RPV), the reactor cavity and RCCS. Unlike the previous study [2], a portion of the reactor cavity, which extends beyond RCCS to the concrete cavity wall, is removed from the present computational domain because the contribution of that wall on the entire heat transfer phenomenon for RCCS was found to be negligible.

To simplify the simulation and to reduce the total calculation time, an axisymmetric assumption is applied to the RCCS geometry. Under this assumption, 292 RCCS tubes are changed into a single annulus cylinder. In Case A, the RCCS has the same inside and outside

radii with the PMR600 design. In Case B, the outside radius of the RCCS annulus is reduced to match the flow area with the design. The difference of the cross-sectional shape between the square duct and the annulus cylinder causes the different flow resistance. To give the same pressure drop with the design, the outside radius of Case C is further reduced by an adjustment after using Idelchik's the friction loss data [3]. Table I shows the summary of three RCCS configurations in the study. The radius is measured from the reactor center.

Each case has a different RCCS flow area, so that the resistance of the RCCS flow path is different from each other. To give the same initial mass flow rates of RCCS for three cases, a pressure jump condition is applied in the middle of the RCCS chimney for each case. The chimney wall above the reactor cavity is assumed to be a frictionless wall. The values of the pressure jumps were adjusted after several steady calculations.

As was used in the previous study, FLUENT [4], was chosen as a CFD tools for this study. The discrete ordinates (DO) radiation model [5] was used to account for the radiation heat transfer. To use the DO model, we

Table I: RCCS configurations in computational domains.

	Case A	Case B	Case C
Outside Radius (m)	4.9712	4.8250	4.7921
Inside Radius (m)	4.7268	4.7268	4.7268
Width (m)	0.2444	0.0982	0.0653
Cross-Sectional Area (m ²)	7.4485	2.9465	1.9530

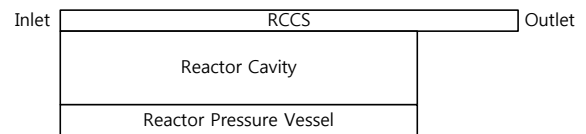


Fig. 1. Schematic diagram of the computational domain.

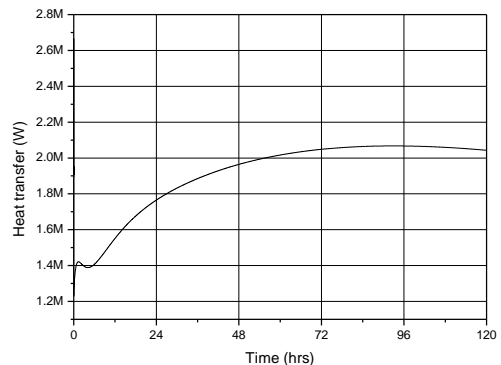


Fig. 2. Time variation of RPV wall heat transfer rate.

chose 7 for the numbers of both divisions and 5×5 for the pixelation. The turbulence model is the RNG $k-\epsilon$ model and the enhanced wall function is provided the boundary condition for the turbulence quantities.

The inlet and outlet boundary conditions are the pressure boundary conditions. The temperature and pressure of the inlet boundary condition are 45°C and 1 bar, respectively. Variation of air properties due to the temperature change was considered. Walls in the domain have properties of steel, which has an emissivity of 0.8.

To simulate the LPCC accident, the unsteady calculation was conducted. The time history of the heat flux, which was obtained by the GAMMA+ calculation, is assigned to the RPV inside wall as a boundary condition (Fig. 2). The time step was selected to be 10 seconds.

2.2 Results

Fig. 3 shows the estimated RCCS mass flow rates. Even though the mass flow rates of RCCS at the initial state are the same, the behaviors of three cases are different. Case C is the most similar to the GAMMA+ among the three cases. After 48 hours, Case A and C estimate the better mass flow rates than Case B does. However, the differences between the estimations are less than 2%. Because of this and the fact that the heat transfers from the RPV wall are the same in all cases, the differences between estimated average temperatures of the RCCS outlet flow are less than 5 K.

The maximum temperature in the RPV wall, which is very important factor to judge whether the design meets its goal, is shown in Fig. 4. All cases estimate higher temperatures than the GAMMA+ results. Case A estimates about 120 K higher temperature than the GAMMA+ results. Case C shows an estimation of about 30 K higher.

The most similar result of the maximum temperature in the RCCS tube walls is obtained by Case B. Case A estimates about 150 K higher maximum RCCS tube wall temperature than GAMMA+. The result of Case C shows about 50 K lower temperature.

The reduced width of the assumed RCCS annulus gives the higher Reynolds number when the mass flow rates are the same.

$$\text{Re} = \frac{VD_h}{\nu} = \frac{\dot{m}D_h}{\mu A} = \frac{4\dot{m}}{\pi(D_o + D_i)\mu} \quad (1)$$

Case C has the highest heat transfer coefficient inside RCCS of Case C due to the highest Reynolds number. This means that Case C estimates the lowest RCCS tube wall temperature as was mentioned above. Because most of the heat transfer is made by radiation, the low RCCS tube wall temperature means the low RPV wall temperature under the same heat transfer rate from the RPV wall. This reasoning explains the estimated results shown in Fig. 4.

3. Concluding Remarks.

The unsteady simulations of RCCS under LPCC accident were performed by CFD using the axisymmetric assumption. The changed shape of the RCCS tube due to the assumption alters the heat transfer phenomena. The estimated results showed that cases of the same cross-sectional area and the same pressure drop with the design give better results than a case with the same outer radius with the design. Furthermore, it is possible to judge that a case with the same pressure drop (Case C) is the most suitable one for estimating the RCCS performance. To verify this, it is further required to perform simulations of other accidents in the future.

REFERENCES

- [1] N.-I. Tak, LPCC data for the FLUENT simulation, Internal communication.
- [2] S. H. Kim, N.-I. Tak, M.-H. Kim, Comparison of Axisymmetric and 3D Simulations of the Heat Transfer in RCCS, KNS Autumn Meeting, PyeongChang, Korea, 2008.
- [3] I. E. Idelchik, Handbook of Hydraulic Resistance, 3th ed., Begell House, 1996.
- [4] FLUENT User's guide, FLUENT Inc., 2006.
- [5] E. H. Chui, G. D. Raithby, Computation of Radiant Heat Transfer on a Non-Orthogonal Mesh Using the Finite-Volume Method, Numerical Heat Transfer, Part B, Vol. 23, p. 269, 1993.

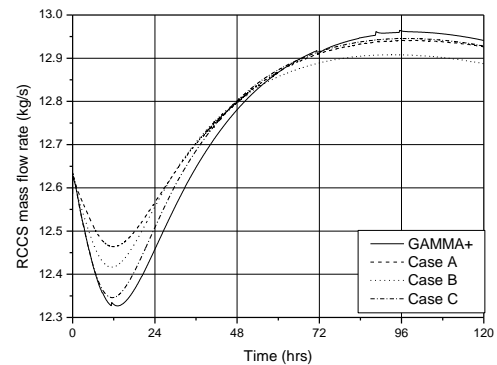


Fig. 3. RCCS mass flow rate.

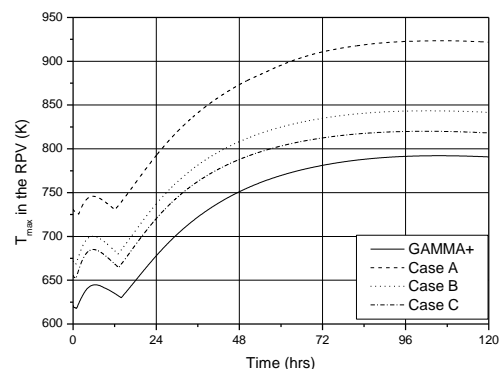


Fig. 4. Maximum temperature in the RPV.